Closing the loop on impulsivity via nucleus accumbens delta-band activity in mice and man

Hemmings Wu[a,1], Kai J. Miller[a,1], Zack Blumenfeld[b], Nolan R. Williams[c], Vinod K. Ravikumar[a], Karen E. Lee[a], Bina Kakusa[a], Matthew D. Sacchet[c], Max Wintermark[d], Daniel J. Christoffel[e], Brian K. Rutt[d], Helen Bronte-Stewart[a,b], Brian Knutson[f], Robert C. Malenka[e,2], and Casey H. Halpern[a,2]

[a]Department of Neurosurgery, Stanford University, Stanford, CA 94305; [b]Department of Neurology and Neurological Sciences, Stanford University, Stanford, CA 94305; [c]Department of Psychiatry and Behavioral Sciences, Stanford University, Stanford, CA 94305; [d]Department of Radiology, Stanford University, Stanford, CA 94305; [e]Nancy Pritzker Laboratory, Department of Psychiatry and Behavioral Sciences, Stanford University, Stanford, CA 94305; and [f]Department of Psychology, Stanford University, Stanford, CA 94305

Reward hypersensitization is a common feature of neuropsychiatric disorders, manifesting as impulsivity for anticipated incentives. Temporally specific changes in activity within the nucleus accumbens (NAc), which occur during anticipatory periods preceding consummatory behavior, represent a critical opportunity for intervention. However, no available therapy is capable of automatically sensing and therapeutically responding to this vulnerable moment in time when anticipation-related neural signals may be present. To identify translatable biomarkers for an off-the-shelf responsive neurostimulation system, we record local field potentials from the NAc of mice and a human anticipating conventional rewards. We find increased power in 1- to 4-Hz oscillations predominate during reward anticipation, which can effectively trigger neurostimulation that reduces consummatory behavior in mice sensitized to highly palatable food. Similar oscillations are present in human NAc during reward anticipation, highlighting the translational potential of our findings in the development of a treatment for a major unmet need.

deep brain stimulation | nucleus accumbens | delta band | closed loop | reward

Impulsivity is one of the most pervasive and disabling features common to many disorders of the brain (1–3). Heightened responsivity in the nucleus accumbens (NAc) during anticipation of a rewarding stimulus predisposes to impulsive behavior, which can have severe implications for development of maladaptive behaviors (4–8). Notably, electrophysiological, neurochemical, and functional neuroimaging correlates have been reported in multiple species during brief windows of anticipation (5, 9–13). These correlates (or biomarkers) that precede a "moment of weakness" have potential to inform a therapeutic to deliver a time-sensitive intervention.

Recently, a responsive neurostimulation (RNS) system was approved by the US Food and Drug Administration for adjunctive treatment of partial onset seizures (14). This intracranial closed-loop system has proven capable of detecting epileptiform activity and preventing propagation by responsively delivering electrical stimulation directly to the seizure onset zone. Here, we examine the potential for RNS to intervene during a vulnerable period immediately preceding receipt of highly rewarding stimuli, an undertaking that has immediate translational potential given the availability of this system. We leveraged the finding that electrically stimulating the NAc in mice anticipating a food reward effectively attenuates binge-eating behavior (15). To "close the loop" on this intervention using an automatic stimulatory system, however, the identification, characterization, and refinement of an anticipatory biomarker are critical next steps.

Given that the currently approved RNS system is limited to local field potential (LFP) recordings due to its implanted depth macroelectrodes' spatial resolution, we make LFP recordings from the mouse and human NAc during a period of reward anticipation, and find prominent delta oscillations elicited during anticipation of a highly rewarding stimulus. Multiunit analysis reveals strong correlations between delta oscillations and unit activities in the NAc. Utilizing this translational biomarker as a trigger, RNS blocked binge eating in mice with remarkable behavioral specificity, thereby taking the first critical step toward the development of a targeted intervention for neuropsychiatric patients suffering from hypersensitivity to pathological motivations.

Results

Increase in NAc Delta-Range Field Potentials Precedes Binge Eating in Mice. Multielectrode arrays were implanted into the NAc of mice (n = 6) (Fig. 1 A–D). Following a 1-wk recovery period, these mice were put on a protocol of 1-h daily exposure to high fat (HF) (standard house chow ad libitum) known to induce binge-like eating behavior (defined as consumption of >25% of daily caloric intake from HF; Fig. 1 E–G). Given prior reports across species of changes in NAc cell firing during reward anticipation (13, 16, 17), mouse NAc LFPs were recorded daily for 2 h, 1 h before and 1 h during exposure to HF food. All mice reached criterion for stable binge eating by day 10 (<10% variation across 3 consecutive days) (15). Power spectral density analyses of NAc LFPs averaged across mice immediately before HF intake on days 0 and 10 were carried out. As a control, identical analyses were performed immediately before the mice ingested standard chow (Fig. 2 A–C). Because our goal was to interrupt a brief vulnerable window in time immediately before a pathological impulse such as a binge-eating episode, we used 2-s windows across a 4-s epoch, which covered from 2 s before to 2 s after the onset of a binge.

Significance

We reveal prominent delta oscillations in the nucleus accumbens preceding food reward in mice and use them to guide responsive neurostimulation to suppress binge-like behavior. Similar electrographic signatures are observed in human nucleus accumbens during reward anticipation as well, suggesting their translational potential in the development of a treatment for loss of impulse control in obesity and perhaps additional brain disorders.

Fig. 1. Schematic of the animal experiment, histology, electrode design, and high-fat (HF) intake summary. (*A*) Schematic of the experimental design: electrode implantation, followed by recovery period (7 d), 1-h daily HF access (days 0–18), and intervention period (days 11–18). (*B–D*) Histology examination revealing the implant locations, and design of the eight-contact multielectrode array, which had six designated recording contacts (in blue/green) and two designated stimulating contacts (in red). (*E–G*) Binge-like behavior developed and stabilized by day 10 of 1-h daily HF exposure, indicated by significant increase in daily HF intake with >25% of daily caloric intake in 1 h. *$P < 0.05$.

The most robust change in LFPs was increased power in very-low–frequency (delta) oscillations once binge eating developed on day 10 immediately before HF intake (Fig. 2 *D–H*). Mean time–frequency spectrograms and comparison of individual frequency bands (delta, 1–4 Hz; alpha, 4–8 Hz; theta, 8–12 Hz; beta, 12–30 Hz; gamma, 30–50 Hz) confirmed that the only statistically significant change in spectral power occurred in the delta frequency range immediately before HF intake after the development of binge-like behavior, compared with baseline (day 0) HF and chow control (delta: $F = 6.165$, $P < 0.001$; Tukey's post hoc test: chow vs. day 0 HF, n.s.; chow vs. day 10 HF, $P < 0.01$; day 0 HF vs. day 10 HF, $P < 0.01$; Fig. 2*H*; alpha, theta, beta, and gamma, chow vs. day 10 HF, n.s.). This increase in power in the delta range was not detected immediately before chow intake, suggesting it was not related to movement or bite artifact. (Movie S1 illustrates increased power in the delta band during HF intake.)

We next compared the delta power immediately before HF consumption on day 10 with that during the entire 1-h exposure to HF. NAc delta oscillations normalized to the entire 1-h period of HF exposure revealed a 30% increase in power during the 2-s window before onset of HF consumption (Fig. 2*I*). Analysis of delta power peak distribution revealed a peak at ~1 s before the onset of HF consumption (Fig. 2*J*). To further test whether the increase in delta power was specific for this highly appetitive food, we recorded LFPs immediately before the interaction of the experimental mice with a novel juvenile, an appetitive experience with a finite, definable onset (Fig. 2*K*). Delta power was significantly lower before the onset of juvenile interaction
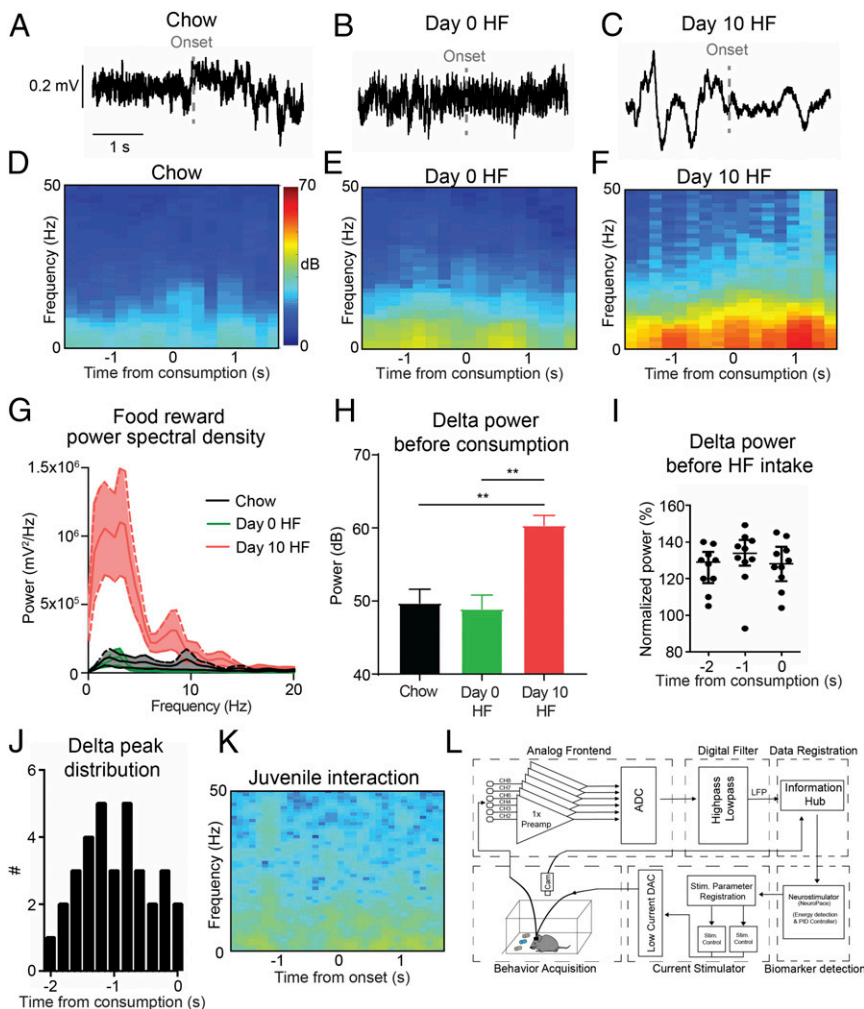
Fig. 2. Raw local field potentials (LFPs), power spectral density, time–frequency analyses of the nucleus accumbens (NAc) LFPs, delta power characterization, and system block diagram of the RNS setup. (*A–C*) Raw LFP samples are shown during the onset (dotted gray line) of house chow as a control and high-fat (HF) consumption on days 0 and 10 (before and after the development of binge-like behavior, respectively). (*D–F*) Mean power spectrogram of NAc LFPs immediately before and after the onset of chow and HF consumption on days 0 and 10. (*G*) Power spectral density analysis of NAc LFPs immediately before (2-s window) chow and HF intake on days 0 and 10, averaged across individual mice, revealing higher power in low-frequency oscillations immediately before the onset of HF intake on day 10. (*H*) Mean delta power significantly increased immediately before the onset of HF intake on day 10 compared with HF intake on day 0 and chow intake. (*I*) Delta power percent change over baseline during the onset of HF consumption on day 10 (normalized to the 1-h period of HF exposure). (*J*) Delta power peak distribution before the onset HF consumption on day 10. (*K*) Mean power spectrogram of NAc LFP during the onset of juvenile interaction. (*L*) System block diagram of the RNS setup, which consisted of a 1× follower cable for unit amplification, a headstage for analog/digital conversion, a digital filter, a computer for synchronizing neural electrophysiological and behavioral data, a prototype biomarker detector (Neurostimulator; model RNS-300; NeuroPace), a constant-current stimulator, and a charge-coupled device camera for synchronized behavioral recording. **$P < 0.01$. See also Fig. S1 and Movie S1.
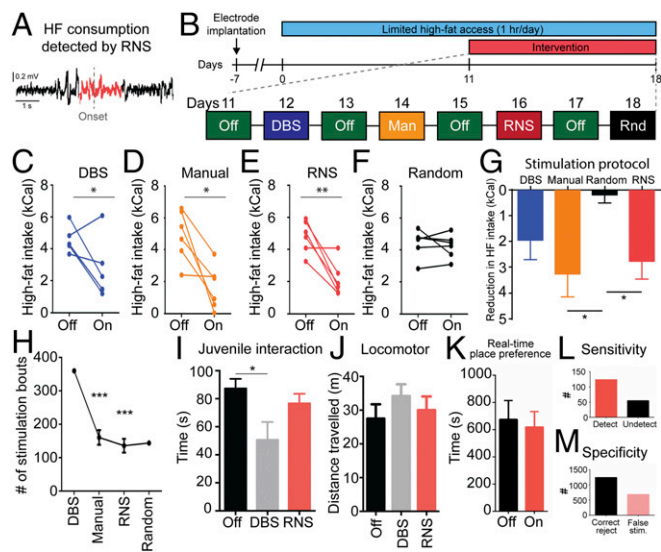
Fig. 3. Schematic of the intervention period during 1-h daily high-fat (HF) exposure in mice, and result summary of different electrical stimulation protocols on HF intake and juvenile interaction. (A) Representative nucleus accumbens (NAc) LFP delta oscillations (in red) at the onset of HF intake detected by the integrated responsive neurostimulation (RNS) system. (B) Schematic of the intervention period. Each intervention session [deep brain stimulation (DBS), manually triggered stimulation (Man), responsive neurostimulation (RNS), randomly applied stimulation (Rnd)] was followed by one washout session (Off). (C–F) The effects of different stimulation protocols on HF consumption. DBS, Man, and RNS significantly reduced HF intake. (G) Reduction in HF intake induced by DBS, manually triggered stimulation, RNS, and randomly applied stimulation, compared with off stimulation. The reduction in HF intake induced by the manually triggered stimulation and RNS was significantly higher than randomly applied stimulation. (H) The number of stimulations bouts (1 bout = 10 s) delivered during Man and RNS were significantly lower than DBS. (I) DBS of the NAc significantly reduced juvenile interaction time, while RNS showed no effect on this behavior. (J) Neither DBS nor RNS of the NAc during HF exposure altered locomotor activity. (K) Real-time place preference test suggested that NAc stimulation was neither rewarding nor aversive. (L and M) Sensitivity and specificity of delta biomarker on RNS day in all six mice. In total, there were 179 HF pellet approaches, of which 124 were detected by the RNS system (sensitivity, 0.693). There were also 1,241 correct rejections (stimulation off when no HF approach occurred) and 685 stimulations triggered when no HF approaches were observed (false stimulation; specificity, 0.644). *$P < 0.05$, **$P < 0.01$, and ***$P < 0.001$. See also Fig. S2 and Movie S2.

compared with the time period before onset of HF intake [$T_{(35)} = 2.719$, $P < 0.05$; Fig. S1]. Together, these results suggest that an increase in delta power in LFPs recorded from the NAc precede intake of HF in binge-eating mice and therefore may be a useful biomarker to trigger RNS.

Delta Oscillations as a Biomarker for RNS. Based on the previous findings, we assessed whether a delta-power threshold could serve as a biomarker to optimize RNS to attenuate HF intake in mice. The closed-loop system (Fig. 2L) was set to trigger whenever delta power exceeded a predefined threshold based on delta peak distribution and power analyses (a threshold of 20% higher than baseline delta power was used, or 1 SD below the mean power immediately before the onset of HF intake; Fig. 2I). When this threshold was reached, electrodes delivered a bipolar, biphasic, 0.1-mA stimulation at 130 Hz for 10 s (Fig. 3A). We compared the efficacy of RNS with that of other neurostimulation protocols in the same experimental animals. Specifically, we also tested (i) continuous electrical stimulation during the entire 1-h exposure to HF, a pattern of stimulation commonly referred to as deep brain stimulation (DBS) (130 Hz, 0.1 mA, bipolar, biphasic); (ii) manually triggered stimulation

during which an experimenter remotely observed the subjects' behavior via video monitoring and triggered electrical stimulation (130 Hz, 0.1 mA, 10 s, bipolar, biphasic stimulation) at the immediate onset of HF consumption; and (iii) random stimulation during which bouts of stimulation (130 Hz, 0.1 mA, 10 s, bipolar, biphasic stimulation) were delivered randomly throughout the entire 1-h HF exposure such that the total number of stimulation bouts matched that delivered during the RNS protocols.

To ensure that caloric intake from HF returned to baseline in-between the stimulation days, each session was followed by a stimulation-off period (Fig. 3B). All of the stimulation protocols significantly reduced HF intake except random stimulation [Fig. 3 C–F; DBS $T_{(5)} = 2.58$, $P < 0.05$; manual $T_{(5)} = 3.75$, $P < 0.05$; RNS $T_{(5)} = 4.29$, $P < 0.01$; random $T_{(5)} = 0.62$, $P = 0.56$]. At the end of these experiments, we repeated another session of RNS, which reproduced the previously seen significant decrease in HF intake [$T_{(5)} = 3.999$, $P < 0.01$; Fig. S2A]. We compared the reduction of HF intake between each stimulation protocol and found that the reductions in HF intake induced by manual stimulation and RNS were significantly more robust than random stimulation [sphericity assumed, $F_{(4)} = 7.034$, $P < 0.01$; post hoc: Manual vs. Random, $P = 0.042$; RNS vs. Random, $P = 0.029$; DBS vs. Random, DBS vs. Manual, DBS vs. RNS, Manual vs. RNS, n.s., Bonferroni corrected; Fig. 3G]. Furthermore, the number of bouts of stimulation used for manual and RNS were significantly lower than DBS [$F_{(1.566,7.813)} = 65.80$, $P < 0.0001$; post hoc: DBS vs. Manual, $P < 0.0001$; DBS vs. RNS, $P < 0.0001$; RNS vs. Manual, n.s.; Tukey's correction applied; Fig. 3H]. (Movie S2 demonstrates RNS triggered by increased delta oscillations before HF intake.)

We conducted a number of additional behavioral assays to determine whether RNS of the NAc might have detrimental side effects. While DBS of the NAc significantly reduced the time spent socially interacting in a juvenile interaction task, RNS using the same delta-band power threshold had no significant effect on interaction time [$F_{(2,21)} = 4.557$, $P < 0.05$; post hoc: Off vs. DBS, $P < 0.05$; Off vs. RNS and RNS vs. DBS, n.s.; Tukey's correction applied; Fig. 3I]. The number of electrical stimulation bouts during RNS was again significantly lower than DBS [$T_{(5)} = 16.15$, $P < 0.0001$]. Spontaneous locomotor behavior during the 1-h daily HF exposure protocol was not affected by DBS nor RNS [$F_{(1.699,8.493)} = 0.891$, $P = 0.429$; Fig. 3J]. Furthermore, NAc stimulation (130-Hz, 0.1-mA, continuous, bipolar, biphasic stimulation) did not induce real-time place preference [$T_{(5)} = 0.2283$, $P = 0.8285$; Fig. 3K]. These results suggest that RNS of the NAc is neither reinforcing nor aversive, and its effects can block consumption of HF food while sparing normal locomotor and social behaviors. We also investigated the sensitivity and specificity of delta oscillations as a biomarker for food reward anticipation by reviewing the videotaped behavior and determining when bouts of electrical stimulation triggered during RNS occurred. Out of a total of 179 HF pellet approaches, 124 were detected by the RNS device such that stimulation was triggered (sensitivity, 0.693; Fig. 3L). There were also 1,241 correct rejections (stimulation withheld when no HF approach occurred) and 685 stimulations triggered when no pellet approach occurred (specificity, 0.644; Fig. 3M). Last, we found that NAc DBS had no significant effect on 24-h chow consumption (Fig. S2B).

To investigate the source of delta oscillations in the NAc during HF consumption in mice, we searched for the occurrence of single-unit activity in the LFP recordings. We identified one type of spike shape consistently (Fig. 4A), which appeared significantly more frequently on day 10 during HF consumption when binge eating was prominent [$F_{(2,12)} = 5.221$, $P < 0.05$; post hoc: chow vs. day 0 HF, n.s.; chow vs. day 10 HF, $P < 0.1$; day 0 HF vs. day 10 HF, $P < 0.05$; Tukey corrected; Fig. 4 B and C]. The delta spike–field coupling, the strength of coupling between spike times and the phase of LFP at delta frequency range, was significantly higher on day 10 immediately before and during HF consumption [$F_{(2,12)} = 8.102$, $P < 0.01$; post hoc: chow vs. day
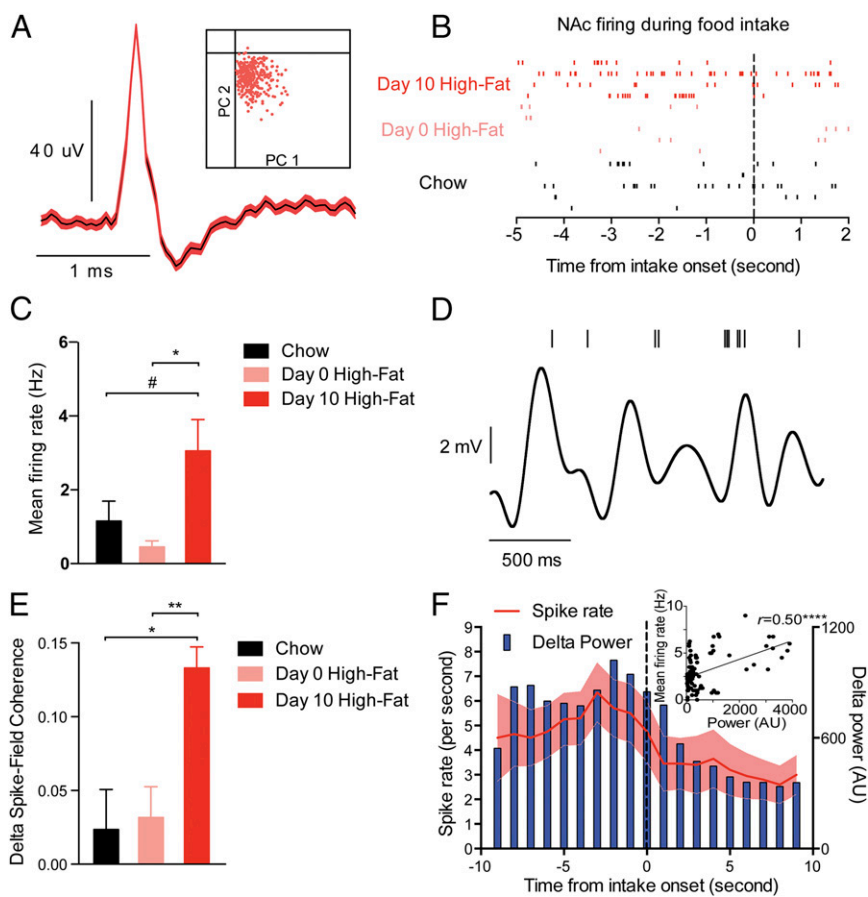
Fig. 4. Multiunit and coherence analyses. (*A*) Identification, principal-component (PC) analysis, and average waveforms of nucleus accumbens (NAc) neurons recorded on day 10 during HF intake. (*B*) Raster plot of NAc firing represented for each trial under different conditions. (*C*) NAc spike rate on day 10 during HF intake was significantly higher than chow and day 0 HF intake. (*D*) Representative example of NAc LFPs (*Bottom*) and unit activities (*Top*), showing phase synchrony with low-frequency oscillations. (*E*) Delta spike–field coupling revealed that the coherence on day 10 during HF intake was significantly higher than chow and day 0 HF intake. (*F*) NAc spike rate significantly correlated with delta power on day 10 during HF intake. $^{\#}P < 0.1$, $*P < 0.05$, $**P < 0.01$, and $****P < 0.0001$.

0 HF, n.s.; chow vs. day 10 HF, $P < 0.05$; day 0 HF vs. day 10 HF, $P < 0.05$; Tukey corrected; Fig. 4 *D* and *E*]. Last, the spike rate significantly correlated with delta power on day 10 immediately before and during HF consumption (Pearson $r = 0.50$, $P < 0.0001$; Fig. 4*F*).

fMRI Activity and Delta Oscillations in Human NAc During Reward Anticipation. To evaluate the translational potential of delta-range field potentials providing physiologic, real-time optimization for RNS in human patients suffering from impulsivity, we recorded intraoperative LFPs from the NAc in a human subject suffering from intractable obsessive-compulsive disorder during a period of reward anticipation analogous to the phase of food reward anticipation examined in mice. Specifically, because in the operating room food rewards could not be provided, we instead elicited anticipation of monetary rewards with a well-established neuroimaging task [i.e., the monetary incentive delay (MID) task]. During each trial of the MID task, a subject sees a visual cue indicating that they will gain or avoid losing an indicated monetary incentive (reward or punishment) by subsequently pressing a button in response to a rapidly presented target. This task allows researchers to distinguish neural responses during different stages of reward processing, including reward anticipation and outcomes (10) (Fig. 5*A*).

Before surgery during a diagnostic magnetic resonance imaging (MRI) scan, fMRI revealed a significant increase in blood oxygen level-dependent (BOLD) signal in the NAc during anticipation of high monetary reward [high reward:baseline, $T_{(17)} = 3.23$, $P < 0.01$, uncorrected; low reward:baseline, high punishment:baseline, low punishment:baseline, n.s.; Fig. 5 *B* and *C*; summary of head movement shown in Fig. S3*A*, demonstrating <1 mm of head movement]. This finding replicated previous reports using normal subjects and corroborates a well-established involvement of the human NAc during reward anticipation (18).

LFPs were recorded via an implanted quadripolar electrode (3389; Medtronic) in the NAc, the location of which was defined by merging a postoperative computed tomography scan of the head to a preoperative 7-T MRI scan using gray matter nulled sequences that indicate precise white matter–gray matter boundaries (Fig. 5*D*). Power spectral density analysis of NAc LFPs during no reward and high reward anticipation (Fig. 5 *E–H*) revealed an increase in delta power during the anticipation period for high reward compared with no reward in the most ventral channel [Fig. 5*H*: $F_{(4,67)} = 3.514$, $P < 0.05$, post hoc: high reward vs. baseline, $P < 0.01$; Tukey's correction applied]. Head and limb movement during intraoperative LFP recordings (Fig. S3*B*) indicated that there was very little detectable movement. Comparison of delta-power measurements during anticipation of high punishments, low punishments, and low rewards normalized to baseline revealed significant increase during anticipation of high reward vs. low punishment (Fig. 5*I* and Fig. S4). We also investigated the correlation between NAc LFP and unit activity during MID task, and found selective phase-locking of spikes to the peak (phase 0) of the delta (2- to 3-Hz) oscillations (Fig. S5).

Discussion

We have demonstrated that anticipation of a large, HF food reward increases delta oscillatory power in the NAc in mice, and preliminary findings from a single human subject support the translatability of this potential biomarker for RNS. In sated mice exhibiting binge-eating behavior, strong delta oscillations are detected 2 s before consuming food reward, but not before intake of house chow. This increase in delta power is not observed before or during general locomotor behavior or social interaction, and is positively correlated with unit activity in the NAc. Using a threshold in delta-band power as a biomarker to trigger delivery of a brief train of high-frequency electrical stimulation pulses to the NAc resulted in significant attenuation
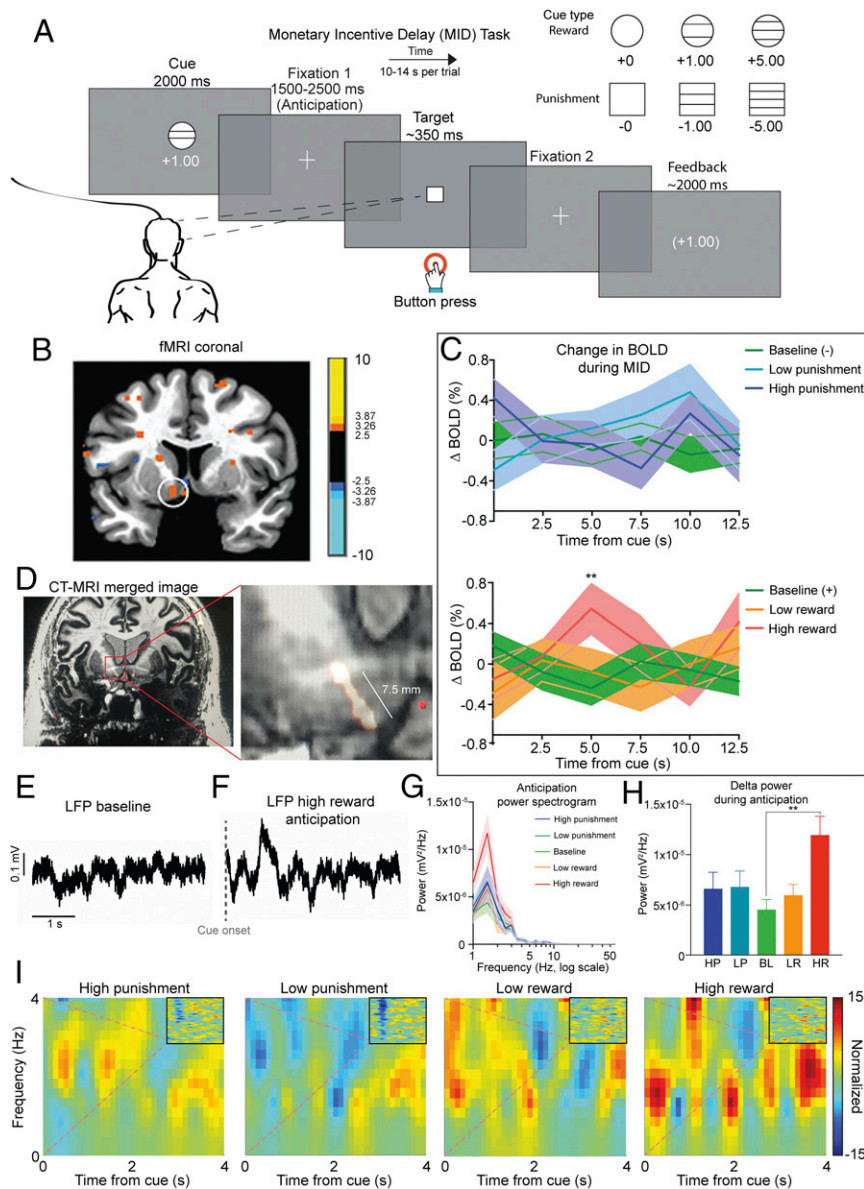
Fig. 5. Schematic of functional neuroimaging and local field potentials (LFPs) recording during the monetary incentive delay (MID) task in human subject. (*A*) Schematic of the MID task, which consists of cue onset, anticipation phase, target onset, and outcome phase. (*B*) Functional magnetic resonance imaging (fMRI) showing area activated by gain vs. nongain anticipation in the nucleus accumbens (NAc) (white circle; $Z > 2.54$; cluster, four 3-mm cubic voxels). (*C*) Blood oxygen level-dependent (BOLD) signal changes during MID task extracted from activated voxels in the left NAc averaged by condition, indicating NAc activation during high reward anticipation compared with baseline [high reward:baseline, $T_{(17)} = 3.23$, $P < 0.01$, uncorrected; low reward:baseline, high punishment:baseline, low punishment:baseline, n.s.]. (*D*) Electrode contact locations in the NAc for LFP recording using preoperative 7-T MRI merged with postoperative computed tomography scan. Coronal view (trajectory view not shown) demonstrates most posterior aspect of electrode trajectory with the following entry anterior–posterior commissure coordinates: $x = 41.31$, $y = 43.39$, $z = 43.59$; 34.2° from midsagittal plane; 60.3° from axial plane; and coordinates for the ventral-most extent of the recording lead: $x = 6.03$, $y = 15.07$, $z = -6.60$. The measurement of 7.5 mm indicates the span of the lead. (*E* and *F*) Raw LFPs during baseline and anticipation of high reward. (*G*) Power density analysis indicating delta range as the frequency region of interest during anticipation period. (*H*) Power density analysis revealing significant increase in delta power during anticipation of high reward compared with baseline. (*I*) Normalized NAc LFP power spectrogram (averaged across individual trials), indicating increased delta band (1- to 4-Hz) power during anticipation of high reward (*Insets*: frequency range from 0 to 50 Hz). **$P < 0.01$. BL, baseline; HP, high punishment; HR, high reward; LP, low punishment; LR, low reward. See also Figs. S3–S5.

of HF intake. The effectiveness of this RNS was reproducible and behaviorally specific. Namely, utilizing power in the delta band as a trigger for RNS did not interfere with social interaction or locomotor behaviors. Moreover, the number of stimulation bouts delivered during RNS was significantly lower than DBS to achieve the same reduction in HF intake. Stimulation of the NAc was not reinforcing or aversive as assayed by a real-time place preference protocol, suggesting that stimulation-induced blockade of HF intake was not substituting for the anticipated food reward or inducing an aversion. Post hoc review of stimulations triggered during RNS revealed that our biomarker settings correctly anticipated about two-thirds of HF binge onsets, while approximately one-quarter of the triggered stimulations were not associated with subsequent binge onset.

To examine the translational potential of our findings, we analyzed NAc LFPs during anticipation of monetary rewards in a human, which, like HF in mice, demonstrably elicits vigorous approach (10). The MID task was used here so that we could examine the human NAc LFPs during a similar brief period of reward anticipation that was studied in mice. Anticipation of large financial incentives are known to reliably increase NAc BOLD signal activity in healthy individuals (18). Because BOLD

activity has been reported to correlate with changes in LFPs (19, 20), we predicted that anticipation of large rewards would induce measurable changes in LFPs in the NAc. Consistent with what is commonly observed in healthy individuals, event-related fMRI in a human subject suffering from severe obsessive-compulsive disorder revealed increased NAc BOLD signal during anticipation of large rewards. Most importantly, NAc LFPs recorded from this subject exhibited an increase in power in the delta band during anticipation of high monetary rewards. These electrophysiological changes echoed those seen in mice anticipating HF reward and importantly was detected by a clinically approved benchtop system. Moreover, the MID task is a good probe of reward anticipation in that it increases positive arousal associated with monetary reward anticipation as has been demonstrated in food reward studies in mice (21, 22).

The illustration of spike–field coupling in humans illustrates that oscillations in the delta range, at the spatial scale of the LFP measured by the high-impedance microelectrode (at ∼200 μm) (23), influence the timing of action potentials in the ventral NAc, although the DBS scale field potential recordings of power change during the reward task (at ∼3.5 mm) (24) are not related in any simple way to the spike field and may differ from the

smaller scale LFP measured by the microelectrode. However, the finding of spike–field coupling does establish the saliency of the delta-range power as a marker of local computation. Together, these findings demonstrate that NAc LFPs carry information relevant to reward anticipation and have the potential to be used as a neural electrographic biomarker to guide RNS treatment for neuropsychiatric disorders exhibiting impulsivity.

RNS remains a therapeutic approach with which clinicians have limited experience. For intractable temporal lobe epilepsy, RNS has proven efficacious in reducing seizure frequency and severity with outcomes that are not only durable but also improve over time (25). Several lines of evidence also suggest that responsive or closed-loop DBS using power in the beta band detected in the subthalamic nucleus across species may be superior to traditional continuous DBS for Parkinson's disease treatment (26–29). Moreover, closed-loop neurostimulation strategies have exhibited promise for other neuropsychiatric diseases, demonstrating the broad potential for this line of research (30).

Our findings provide preliminary evidence that RNS has potential for treating intractable behavioral disorders that have not previously been considered optimal candidates for neurosurgical approaches, including eating disorders, and even obesity and addiction. Undoubtedly, further work will optimize biomarkers of reward anticipation by improving their specificity and sensitivity. We used chow as the primary food control in our study, and social interaction as another behavioral control as this is considered an assay of reward processing in mice. The consequences of exposure to other appetitive stimuli, such as drugs of abuse or sexually receptive partners, will be important to examine to better define the specificity of the LFP biomarkers reported here. Clearly, many more experiments in both animals and humans will be necessary to minimize potential side effects

of RNS and maximize its therapeutic utility. Nevertheless, the fact that mouse and human NAc LFPs exhibit similar changes during reward anticipation suggests that mechanistically driven research in rodents can inform what is eventually done in human subjects. Furthermore, we have demonstrated that the candidate biomarker can be detected using an off-the-shelf, commercially available RNS device, suggesting that rapid progress can be made toward a neurostimulation treatment for patients suffering from intractable, life-threatening impulse control disorders. As human trials are undertaken for novel behavioral indications, systematic plans for monitoring patient subjects by a multidisciplinary team will be critical to best assay the future potential of this intervention.

Materials and Methods

All animal procedures conformed to the NIH *Guide for the Care and Use of Laboratory Animals* (31) and were approved by the Stanford University Administrative Panel on Laboratory Animal Care (APLAC-30216). Clinical investigation was carried out in accordance with a Stanford University IRB-approved protocol (IRB-33146). Informed consent was obtained. See *SI Materials and Methods* for details.

1. Kessler RC, et al. (2005) Lifetime prevalence and age-of-onset distributions of DSM-IV disorders in the National Comorbidity Survey Replication. *Arch Gen Psychiatry* 62: 593–602, and erratum (2005) 62:768.
2. Weintraub D, et al. (2010) Impulse control disorders in Parkinson disease: A cross-sectional study of 3090 patients. *Arch Neurol* 67:589–595.
3. Baxter LR, Jr (2003) Basal ganglia systems in ritualistic social displays: Reptiles and humans; function and illness. *Physiol Behav* 79:451–460.
4. Martin LE, Potts GF (2004) Reward sensitivity in impulsivity. *Neuroreport* 15:1519–1522.
5. Smith CT, et al. (2016) Modulation of impulsivity and reward sensitivity in intertemporal choice by striatal and midbrain dopamine synthesis in healthy adults. *J Neurophysiol* 115:1146–1156.
6. Demos KE, Heatherton TF, Kelley WM (2012) Individual differences in nucleus accumbens activity to food and sexual images predict weight gain and sexual behavior. *J Neurosci* 32:5549–5552.
7. Buckholtz JW, et al. (2010) Mesolimbic dopamine reward system hypersensitivity in individuals with psychopathic traits. *Nat Neurosci* 13:419–421.
8. Dalley JW, Everitt BJ, Robbins TW (2011) Impulsivity, compulsivity, and top-down cognitive control. *Neuron* 69:680–694.
9. Crockett MJ, et al. (2013) Restricting temptations: Neural mechanisms of pre-commitment. *Neuron* 79:391–401.
10. Knutson B, Westdorp A, Kaiser E, Hommer D (2000) FMRI visualization of brain activity during a monetary incentive delay task. *Neuroimage* 12:20–27.
11. Richard JM, Ambroggi F, Janak PH, Fields HL (2016) Ventral pallidum neurons encode incentive value and promote cue-elicited instrumental actions. *Neuron* 90:1165–1173.
12. Roitman MF, Stuber GD, Phillips PE, Wightman RM, Carelli RM (2004) Dopamine operates as a subsecond modulator of food seeking. *J Neurosci* 24:1265–1271.
13. Taha SA, Fields HL (2006) Inhibitions of nucleus accumbens neurons encode a gating signal for reward-directed behavior. *J Neurosci* 26:217–222.
14. Morrell MJ; RNS System in Epilepsy Study Group (2011) Responsive cortical stimulation for the treatment of medically intractable partial epilepsy. *Neurology* 77:1295–1304.
15. Halpern CH, et al. (2013) Amelioration of binge eating by nucleus accumbens shell deep brain stimulation in mice involves D2 receptor modulation. *J Neurosci* 33:7122–7129.
16. Schultz W, Apicella P, Scarnati E, Ljungberg T (1992) Neuronal activity in monkey ventral striatum related to the expectation of reward. *J Neurosci* 12:4595–4610.
17. Carelli RM, Deadwyler SA (1994) A comparison of nucleus accumbens neuronal firing patterns during cocaine self-administration and water reinforcement in rats. *J Neurosci* 14:7735–7746.
18. Knutson B, Wimmer GE, Kuhnen CM, Winkielman P (2008) Nucleus accumbens activation mediates the influence of reward cues on financial risk taking. *Neuroreport* 19:509–513.
19. Magri C, Schridde U, Murayama Y, Panzeri S, Logothetis NK (2012) The amplitude and timing of the BOLD signal reflects the relationship between local field potential power at different frequencies. *J Neurosci* 32:1395–1407.
20. Lu H, et al. (2007) Synchronized delta oscillations correlate with the resting-state functional MRI signal. *Proc Natl Acad Sci USA* 104:18265–18269.
21. Teegarden SL, Bale TL (2007) Decreases in dietary preference produce increased emotionality and risk for dietary relapse. *Biol Psychiatry* 61:1021–1029.
22. Knutson B, Katovich K, Suri G (2014) Inferring affect from fMRI data. *Trends Cogn Sci* 18:422–428.
23. Einevoll GT, Kayser C, Logothetis NK, Panzeri S (2013) Modelling and analysis of local field potentials for studying the function of cortical circuits. *Nat Rev Neurosci* 14:770–785.
24. Lempka SF, McIntyre CC (2013) Theoretical analysis of the local field potential in deep brain stimulation applications. *PLoS One* 8:e59839.
25. Bergey GK, et al. (2015) Long-term treatment with responsive brain stimulation in adults with refractory partial seizures. *Neurology* 84:810–817.
26. Rosin B, et al. (2011) Closed-loop deep brain stimulation is superior in ameliorating parkinsonism. *Neuron* 72:370–384.
27. Wingeier B, et al. (2006) Intra-operative STN DBS attenuates the prominent beta rhythm in the STN in Parkinson's disease. *Exp Neurol* 197:244–251.
28. Little S, et al. (2013) Adaptive deep brain stimulation in advanced Parkinson disease. *Ann Neurol* 74:449–457.
29. Avila I, et al. (2010) Beta frequency synchronization in basal ganglia output during rest and walk in a hemiparkinsonian rat. *Exp Neurol* 221:307–319.
30. Widge AS, Moritz CT (2014) Pre-frontal control of closed-loop limbic neurostimulation by rodents using a brain-computer interface. *J Neural Eng* 11:024001.
31. National Research Council (2011) *Guide for the Care and Use of Laboratory Animals* (National Academies Press, Washington, DC), 8th Ed.